Journal of Ceramic Processing Research. Vol. 26, No. 1, pp. 37~42 (2025)
(Received 31 August 2024, Received in revised form 1 November 2024, Accepted 17 December 2024)
https://doi.org/10.36410/jcpr.2025.26.1.37

J O U R N A L O F
Ceramic Processing Research

Investigation of the Ba doping effect on the dielectric properties of $LaFeO_3$ ceramics

Ziheng Huang, Depeng Wang, Xiaoyu Wu, Wei Li and Weitian Wang*
School of Physics and Electronic Information, Yantai University, Yantai 264005, P.R. China

Ba-doped $LaFeO_3$ [$La_{1-x}Ba_xFeO_3$ ($0 \le x \le 0.4$)] ceramics were synthesized using the solid-state reaction method. The phase purity and structural characteristics were confirmed by X-ray diffraction, revealing that all samples exhibit a cubic structure with a Pm-3m space group. X-ray photoelectron spectroscopy was used to identify the chemical state of the component elements. The dielectric properties and conductivity measurements have been carried out. It was found that doping Ba into the ferrite $LaFeO_3$ resulted in an enhancement of dielectric constant, with the dielectric loss showing Debye-type dipolar relaxation behavior. This behavior is linked to the polarization from small polarons caused by electron hopping between Fe^{2+} and Fe^{3+} ions.

Keywords: Ceramics, Dielectric properties, Conductivity.

Introduction

Oxide materials with high dielectric constants coupled with low losses hold crucial value in the advancement of microelectronics, facilitating the downsizing of electronic components. As opposed to complex oxide structures, the $RFeO_3$ system, where R represents a rare-earth element, offers a simpler framework that is well-suited for investigating properties associated with superior dielectric capabilities. $LaFeO_3$, as a typical perovskite-type material, has attracted considerable attention for its unique physico-chemical properties and susceptibility to significant changes with alterations in their composition [1, 2]. Many research achievements on $LaFeO_3$ have been reported in various state-of-the-art fields such as solid oxide fuel cells, photocatalysis, chemical sensors, magnetic material advancements, and the innovation of electrode materials [3-9].

Furthermore, the cation doping technique has been proved to be an effective method to modify the desirable properties of $LaFeO_3$. Several studies reveal that doping can result in changes in lattice distortions and electronic configuration, which in turn affect the dielectric properties of $LaFeO_3$ [10-13]. Huang et al. reported that the creation of oxygen vacancies in $La_{1-x}Sr_xFeO_3$ nanoparticles were crucial for the charge compensation during the substitution of high-valence cation ions with low-valence ones [14]. Similarly, Cao et al. discovered that $La_{1-x}Na_xFeO_3$ crystals exhibited a dielectric constant as high as 10^5 at low frequencies [15]. Additionally, it was observed by L. H. Omari et al. that the solid solution of $0.97(PbTiO_3)$-$0.03(LaFeO_3)$ showed an optical bandgap of 2.032 eV, indicating it as a potential material for solar cell technologies [16]. Up to now, cation ions with different valence states, such as monovalent elements Na [15], K [17], Ag [18]; divalent elements Pb [19], Sr [20], Zn [21]; trivalent elements Co [22], Cr [23], Al [24]; and tetravalent elements Ti [25] have been reported as dopants entering into $LaFeO_3$ crystal lattice, and their effects on magnetic or electrical and optical properties have been investigated.

However, there are few reports on the dielectric properties of Ba-doped $LaFeO_3$ ceramics. In this work, a seris of $La_{1-x}Ba_xFeO_3$ ceramic samples were synthesized using the solid-state reaction method, and the effect of Ba doping on the dielectric properties of $LaFeO_3$ was investigated. Our results show that the use of Ba ions as A-site dopants contributes to the increase of dielectric constant, which can be explained by the dipolar effect originate from the Fe^{3+}/Fe^{2+} ion pairs.

Experimental Procedure

By employing high-purity chemical reagents La_2O_3 (≥99.9%), Fe_2O_3 (≥99.5%), and $BaCO_3$ (≥99.5%), the $La_{1-x}Ba_xFeO_3$ ceramics were synthesized using the solid-state reaction method. The raw chemical materials were meticulously weighed according to the stoichiometric ratio and thoroughly mixed. Five $La_{1-x}Ba_xFeO_3$ ceramics were prepared with setting x = 0, 0.1, 0.2, 0.3, 0.4, and the corresponding samples were denoted as LBFO0, LBFO1, LBFO2, LBFO3, LBFO4, respectively. The

*Corresponding author:
Tel : +86 13573512787
Fax: +86 535 6901947
E-mail: wtwang@ytu.edu.cn

mixed powders were finely ground, proceeding with a solid-state calcination process at 1350 °C in a muffle furnace for a duration of 6 hours. Subsequently, the derived materials were reground in an agate pestle and mortar for a period of 1 hour, and then pressed into cylindrical pellets of uniform thickness using a pellet press. These pellets were sintered at 1400 °C for 6 h to form ceramic samples. Finally, silver paste was uniformly applied to both sides of the pellets, and silver wires were connected. After thorough drying, the samples were subjected to appropriate characterization and dielectric measurements.

The crystal structure of the prepared samples was investigated using X-ray diffraction (XRD) with CuKα radiation (λ = 1.5418 Å) over a 2θ range of 10°~80°, employing an X'Pert3 Powder diffractometer (PANalytical, The Netherlands). Structural analysis of the XRD data was performed using the General Structure Analysis System (GSAS) and VESTA (JP-Mineral.org, Ibaraki, Japan) software. X-ray photoelectron spectroscopy (XPS) analysis was performed utilizing a monochromatic AlKα X-ray source from the ESCALAB 250Xi, a device manufactured by Thermo Electron Corporation in the USA. To investigate the dielectric properties, a HIOKI 3532-50 LCR HiTester and an HP4194A analyzer were utilized for measurements over a frequency range of 100 Hz to 1 MHz.

Results and Discussions

The XRD patterns of the prepared samples are shown in Fig. 1. All the diffraction patterns demonstrate excellent crystalline quality and the presence of iron-based perovskite phases. The diffraction peaks were confirmed and indexed with the standard reference pattern of $LaFeO_3$ in the Pm-3m space group (PDF#75-0541). No impurities or alternative phases can be detected. With increasing doping concentration, the peaks slightly shifted to lower angles, as shown in Fig. 1(b), indicating

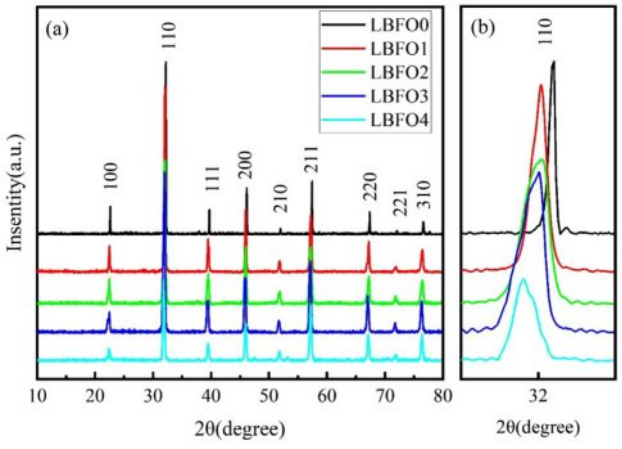

Fig. 1. (a) XRD patterns of the prepared samples, and (b) the enlarged view of the (110) plane.

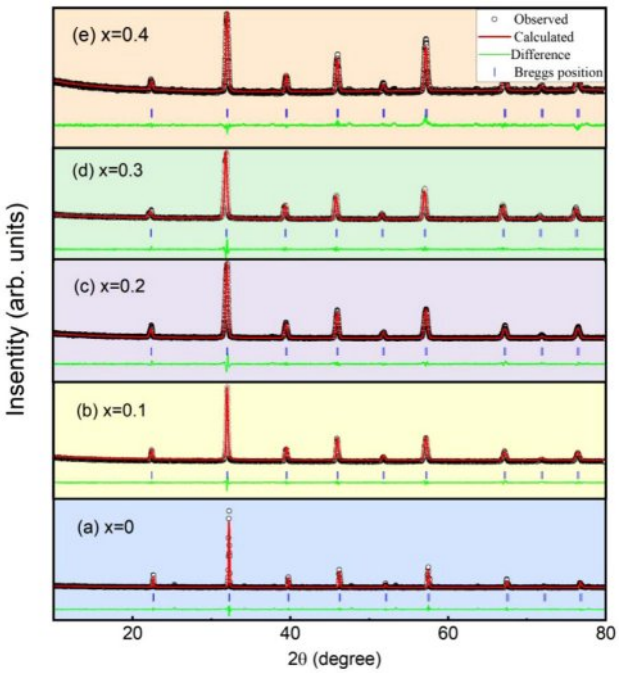

Fig. 2. Rietveld refinement results of the XRD patterns of $La_{1-x}Ba_xFeO_3$, (a) x=0, (b) x=0.1, (c) x=0.2, (d) x=0.3, (e) x=0.4.

an expansion of the lattice parameters. This is mainly because the ionic radius of Ba^{2+} is approximately 135 pm, whereas that of La^{3+} is approximately 103 pm. Doping with larger ions accounts for the low-angle shift of the diffraction peaks.

The Rietveld refinement was carried out using the GSAS program to analyze the XRD data. The refinement results of the five samples are shown in Figs. 2(a-e). All the samples crystallize in cubic perovskite structure with the Pm-3m space group. The lattice parameters for all samples were refined using the least-squares method. The obtained lattice parameters (a, b, c), unit cell volume (V), and reliability factors (R_{wp}, R_p) for different doping concentrations are presented in Table 1. With the increase of doping concentration x, the expansion of lattice parameters and unit cell volume is confirmed.

The chemical state of the component elements of the prepare samples was investigated using XPS analysis. Fig. 3 displays the XPS spectra for LBFO2 as a typical case. The high-resolution scan of the La 2p spectra [Fig. 3(a)] exhibit peaks for La $2p_{5/2}$ and La $2p_{3/2}$ at 883.7 eV and 850.7 eV, respectively, with characteristic satellite peaks in accordance with the standard La^{3+} [26]. The Fe 2p spectra [Fig. 3(b)] display a doublet assigned to $2p_{3/2}$ and $2p_{1/2}$, respectively. The $2p_{3/2}$ peak is resolved into two peaks at 710.7 eV and 713 eV, attributed to Fe^{2+} and Fe^{3+}, respectively. This is in agreement with the reports by Martine Mullet et al. [27], indicating a mixed-valence state of iron in the samples. The Ba 3d high-resolution XPS spectra [Fig. 3(c)] suggest that the Ba ions are in Ba^{2+} states. Generally, doping a lower valence state cation into ABO_3 oxides can lead to the reduction of oxygen

Table 1. Structural parameters of the prepared $La_{1-x}Ba_xFeO_3$ ceramics.

Parameters		Ba concentration				
		0%	10%	20%	30%	40%
Space group		Pm-3m	Pm-3m	Pm-3m	Pm-3m	Pm-3m
Crystal symmetry		Cubic	Cubic	Cubic	Cubic	Cubic
Lattice constants(Å) a=b=c		3.92415	3.93227	3.93349	3.93359	3.93372
Unit cell volume, V(Å)^3		60.427	60.804	60.86	60.865	60.871
Reliability factors	R_p	7.45%	8.26%	6.79%	6.6%	6.74%
	R_{wp}	9.76%	9.63%	8.61%	8.38%	8.8%

ions and the subsequent formation of vacancies [28, 29]. When Ba^{2+} is introduced as a dopant, it substitutes for La^{3+}, leading to charge compensation mechanisms that influence the iron oxidation states. The existing oxygen vacancies provide additional electrons, reducing Fe^{3+} to Fe^{2+}. The relative concentrations of these valence states are calculated to be 34.8% (Fe^{2+}), and 65.2% (Fe^{3+}) for the sample LBFO2. As the concentration of Ba^{2+} increases, more Fe^{3+} ions are reduced to Fe^{2+} to balance the additional positive charge introduced by oxygen vacancies. This results in an increased Fe^{2+}/Fe^{3+} ratio. The transfer of charge carriers between Fe^{2+}-Fe^{3+} ions induces electron-pinned defect-dipoles which align to a varying electric field, resulting in the increased dielectric properties. The oxygen vacancies were confirmed by the O 1s XPS spectra, as shown in Fig. 3(d). The broad peak is deconvoluted into three Gaussian peaks at 529.8 eV, 530.7 eV, and 531.8 eV, which can be ascribed to lattice oxygen, oxygen vacancies, and surface-adsorbed oxygen, respectively. These findings are in line with the results reported by C. C. Wang et al. on $BaFeO_{3-\delta}$ ceramics [30].

The dielectric properties were analyzed over a frequency range of 100 Hz to 1 MHz under the room temperature. The dielectric constant, denoted as ε', was determined using the following equation:

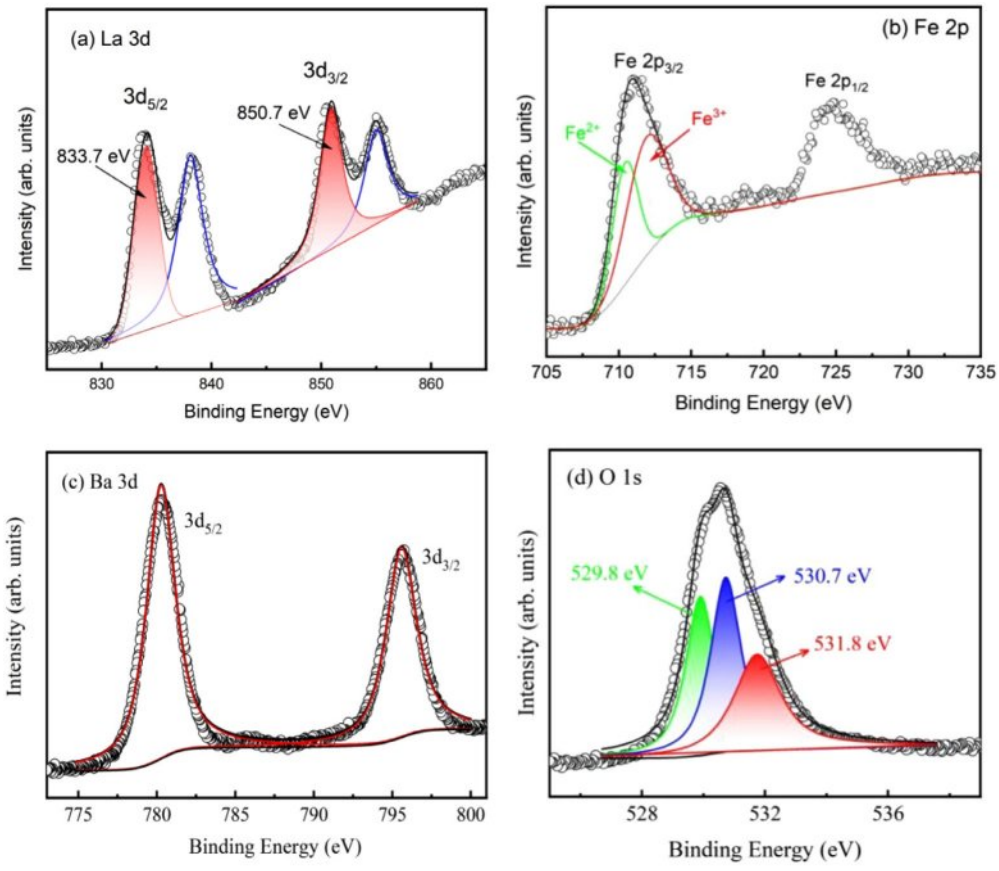

Fig. 3. Typical XPS spectra of (a) La3d, (b) Fe2p, (c) Ba 3d and (d) O1s for the LBFO2 sample.

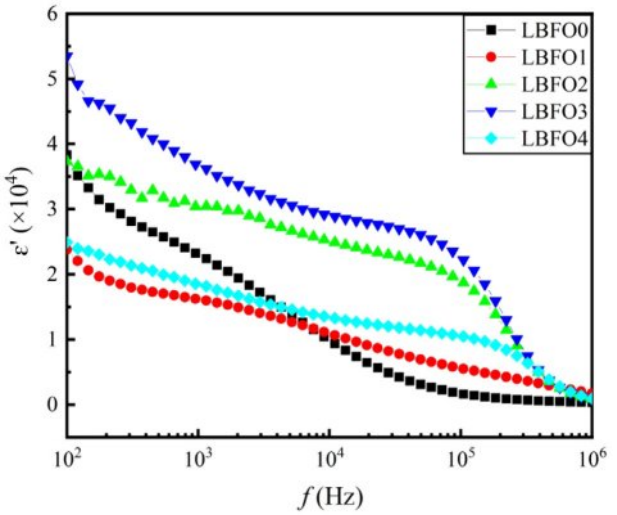

Fig. 4. Frequency dependence of ε' for the prepared samples at room temperature.

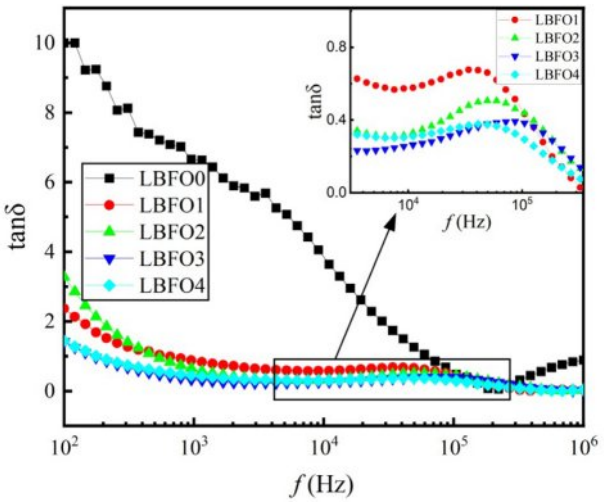

Fig. 5. Frequency dependence of tanδ for the prepared samples at room temperature.

$$\varepsilon' = \frac{C \cdot d}{S \cdot \varepsilon_0} \tag{1}$$

where C represents the capacitance, S is the cross-sectional area of the pellet, d is the thickness of the pellet, and ε_0 is the permittivity of free space. Fig. 4 shows the variation of the dielectric constant ε' with frequency for the prepared samples. At low frequencies ($f < 10^4$ Hz), the dielectric constant is large due to the dipolar polarization in the dielectric material. As frequency increases, the dielectric constant tends to reduce because electron movement may not synchronize with the fluctuations of the external electric field, potentially resulting in saturation and minor alterations [31]. Similar trends have been reported in the dielectric properties of other oxide materials [32, 33].

It is likely that the Ba doping can help to increase the dielectric constant although the values reduce a little in the low-frequency range (f < 5 kHz). This enhancement may originate from the dipolar effect arising from the Fe^{3+}/Fe^{2+} ion pairs, as shown in the XPS analysis (Fig. 3(b)), within the perovskite framework of iron. The transfer of electrons between these ions induces dipolar polarization which aligns the dipoles in response to a varying electric field, resulting in the increased dielectric properties. In addition, the introduction of Ba^{2+} into $LaFeO_3$ structure may also cause distortion of the FeO_6 octahedra, leading to the formation of oxygen vacancies, which could weaken the interaction between the A-site and B-site sublattices, thereby reducing polarization resistance. Therefore, polarization and the dielectric properties increase consequently [34]. Moreover, the presence of oxygen vacancies can lead to the formation of defect dipoles, where the vacancy itself acts as a negative charge center and neighboring atoms or ions redistribute to form a positive charge center. These defect dipoles can align with the external field, contributing to the overall polarization [35, 36].

Figure 5 shows the frequency dependence of tanδ for the prepared samples. It is obvious that when La^{3+} is replaced by Ba^{2+} ions, the curves of samples LBFO1, LBFO2, LBFO3, and LBFO4 exhibit relaxation peaks, leading to a Debye-type dipolar relaxation response. The Debye relaxation is characteristic of a group of non-interacting ideal dipoles that have the same waiting period before transitioning or a set of dipoles that lose energy at a rate proportional to frequency. As is known, dielectric relaxation is influenced by the mobility and alignment of charged species within the material. The presence of Ba^{2+} ions can lead to partial charge transfer or redox reactions and modify the local electric field experienced by Fe^{2+}/Fe^{3+} pairs, influencing their relaxation behaviors. This type of relaxation can be simulated by combining capacitance (C) and resistance (R) in various ways, resulting in a peak frequency of $f_p = (RC)^{-1}$. The peaks in the dielectric loss are indicative of a significant link between the dielectric response and the conduction mechanisms in ferrites [37, 38]. The occurrence of a peak is anticipated when the frequency of electron hopping between Fe^{2+} and Fe^{3+} ions is roughly equivalent to the external field frequency, satisfying the condition $\omega t = 1$, where t is the relaxation time for the hopping process and ω is the angular frequency of the external field [39].

To further investigate the transport mechanism, the conductivity σ of the prepared samples was studied. Fig. 6 shows the results at room temperature. In the low-frequency region, there are almost no noticeable changes for the values of σ. In the high-frequency range, there is a significant increase of conductivity with the increasing frequency. As is known, the conductivity can be described by Mott's law, $\sigma(\omega, T) = \sigma_{dc}(T) + \sigma_{ac}(\omega, T)$, where σ_{dc} and σ_{ac} denote the DC and AC conductivity, respectively. At lower frequencies, the DC conductivity is the dominant

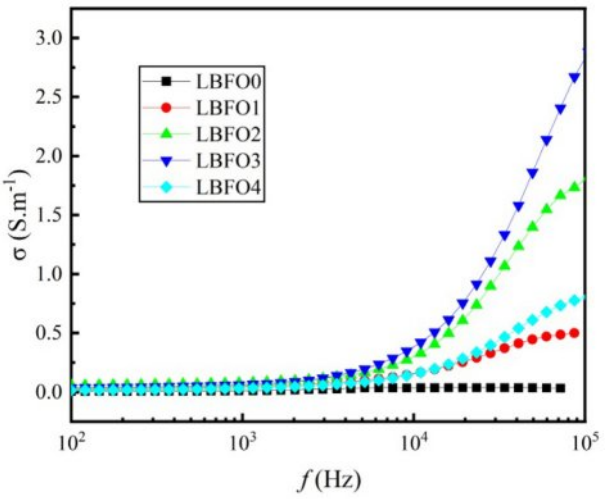

Fig. 6. Frequency dependence of σ for the prepared samples.

process, which remains constant regardless of frequency and is dependent on the mobility of free charge carriers. As the frequency increases, the alternating electric field is applied to the electron hopping between Fe^{2+} and Fe^{3+} ions within the samples, which in turn enhances the AC conductivity. Meanwhile, oxygen vacancies introduce defects acting as traps or donors, which can facilitate the movement of charge carriers. When an external AC field is applied, these defect states can capture and release electrons more readily, enhancing the material's AC conductivity at high frequencies. The improving AC conductivity is responsible for the increased values of σ in the high-frequency range. Similar results have been reported by many literatures [40]. It seems that the introduction of Ba^{2+} can reduce polarization resistance due to the weakening interaction between the A-site and B-site sublattices. Lower polarization resistance leads to higher response times and decreased energy losses, which are favorable for the device performance. The reduction in polarization resistance directly benefits sensors by enhancing sensitivity and improving response time. In the same way, a lower polarization resistance can improves capacitor characteristics through increasing density and efficiency [41].

Conclusion

Ba-doped $LaFeO_3$ ceramics were synthesized using a conventional solid-state method. Different valence state of Fe irons and oxygen defects were revealed. Dielectric measurements suggest that the dielectric constant and loss are influenced by the Ba doping concentration. The doping of Ba^{2+} increases the dielectric constant, results in the Debye-type relaxation peaks. The conductivity data suggest that the observed Debye-type response may be associated with polaronic relaxation due to electron movement between Fe^{2+} and Fe^{3+} ions.

Acknowledgment

This work was supported by the National Natural Science Foundation of China (No. 12374031) and the Graduate Innovation Foundation of Yantai University (No. GGIFYTU2315).

References

1. P. Manimuthu, and C. Venkateswaran, J. Phys. D: Appl. Phys. 45 (2012) 015303.
2. I.R. Shein, V.L. Kozhevnikov, and A.L. Ivanovskii, J. Phys. Chem. Solids. 67 (2006) 1436-1439.
3. A.S. Nesaraj, S. Dheenadayalan, I.A. Raj, and R. Pattabiraman, J. Ceram. Process. Res. 13[5] (2012) 601-606.
4. Q. Zhang and F. Saito, J. Mater. Sci. 36 (2001) 2287-2290.
5. S.L. Bai, B.J. Shi, L.J. Ma, P.C. Yang, Z.Y. Liu, D.Q. Li, and A.F. Chen, Sci. China. Ser. B: Chem. 52[12] (2009) 2106-2113.
6. Z. Dai, C.S. Lee, B.Y. Kim, C.H. Kwak, J.W. Yoon, H.M. Jeong, and J.H. Lee, ACS Appl. Mater. Interfaces. 6[18] (2014) 16217-16226.
7. T. Arakawa, H. Kurachi, and J. Shiokawa, J. Mater. Sci. 20 (1985) 1207-1210.
8. Y. Shimizu, M. Shimabukuro, H. Arai, and T. Seiyama, Chem. Lett. 14[7] (1985) 917-920.
9. G. Martinelli, M.C. Carotta, M. Ferroni, Y. Sadaoka, and E. Traversa, Sens. Actuators B: Chem. 55[2-3] (1999) 99-110.
10. M.M. Arman and M.A. Ahmed, Appl. Phys. A. 128[7] (2022) 554.
11. I. Bhat, S. Husain, W. Khan, and S.I. Patih, Mater. Res. Bull. 48[11] (2013) 4506-4512.
12. M.A. Matin, M.N. Hossain, M.M. Rhaman, F.A. Mozahid, M.A. Ali, M.A. Hakim, and M.F. Lslam, SN Appl. Sci. 1 (2019) 1-8.
13. R.A. Kumar, A. Dutta, P.K. Mukhopadhyay, and T.P. Sinha, J. Alloys Compd. 730 (2018) 201-207.
14. L. Huang, L. Cheng, S. Pan, Y. He, C. Tian, J. Yu, and H. Zhou, Ceram. Int. 46[17] (2020) 27352-27361.
15. E. Cao, Y. Qin, T. Cui, L. Sun, W. Hao, and Y. Zhang, Ceram. Int. 43[10] (2017) 7922-7928.
16. L.H. Omari, H. Lemziouka, M. Haddad, and T. Lamhasni, Mater. Today: Proc. 13 (2019) 1205-1214.
17. M.B. Bellakki and V. Manivannan, Bull. Mater. Sci. 33 (2010) 611-618.
18. M.B. Bellakki, B.J. Kelly, and V. Manivannan, J. Alloys Compd. 489[1] (2010) 64-71.
19. S. Kumar, J. Pal, S. Kaur, R. Kaur, P.D. Babu, M. Singh, and A. Singh, J. Magn. Magn. Mater. 467 (2018) 89-95.
20. Q. Ming, M.D. Nersesyan, A. Wagner, J.T. Pichardson, D. Luss, A.J. Jacobson, and Y.L. Yang, Solid State Ion. 122[1-4] (1999) 113-121.
21. K. Mukhopadhyay, A.S. Mahapatra, and P.K. Chakrabarti, J. Magn. Magn. Mater. 329 (2013) 133-141.
22. I.O. Troyanchuk, D.V. Karpinsky, R. Szymczak, and H. Szymczak, J. Magn. Magn. Mater. 298 (2006) 19-24.
23. A.P.B. Selvadurai, V. Pazhanivelu, C. Jagadeeshwaran, R. Murugaraj, I.P. Muthuselvam, and F.C. Chou, J. Alloys Compd. 646 (2015) 924-931.
24. S. Acharya and P.K. Chakrabarti, Solid State Commun.

150[27-28] (2010) 1234-1237.
25. S. Phokha, S. Hunpratup, S. Pinitsoontorn, B. Putasaeng, S. Rujirawat, and S. Maensiri, Mater. Res. Bull. 67 (2015) 118-125.
26. M.M. Natile, A. Galenda, and A. Glisenti, Surf. Sci. Spectra. 15[1] (2008) 1-13.
27. M. Mullet, V. Khare, and C. Ruby, Surf. Interface Anal. 40[3-4] (2008) 323-328.
28. C. Chen, K. Xu, X. Ji, B. Zhang, and J. Jiang, J. Mater. Chem. A 3[23] (2015) 12461-12467.
29. J.H. Hwang and K.T. Lee, J. Ceram. Process. Res. 19[5] (2018) 372-377
30. R. Ahmed, S.T. Wang, J. Sun, J. Wang, T.Y. Li, Y. Yu, Q.J. Li, and C.C. Wang, Ceram. Int. 45[10] (2019) 13484-13487.
31. K.K. Patankar, P.D. Dombale, V.L. Mathe, S.A. Patil, and R.N. PaTil, Mater. Sci. Eng. B. 87[1] (2001) 53-58.
32. M.A. Ali, M.N.I. Khan, F.U.Z. Chowdhury, S. Akhter, and M.M. Uddin, J. Sci. Res. 7 (2015) 65-75.
33. M.A. Ali, M.M. Uddin, M.N.I. Khan, F.U.Z. Chowdhury, S.M. Hoque, and S.I. Liba, Chin. Phys. B. 26[7] (2017) 077501.
34. K. M. Batoo, and M. S. Ansari, Nanoscale Res. Lett. 7 (2012) 1-14.
35. X. Li, Z. Wang, A. Sasani, A. Baktash, K. Wang, H. Lu, J. You, P. Chen, P. Chen, Y. Bao, S. Zhang , G. Liu, and L. Wang, Nat. Commun. 15 (2024) 9127.
36. H.K. Kim, J.H. Kim, S.H. Lee, H.J. Choi and Y.H. Lee, J. Ceram. Process. Res. 17[7] (2016) 738-741.
37. N. Rezlescu and E. Rezlescu, Solid State Commun. 14[1] (1974) 69-72.
38. K. Iwauchi, Jpn. J. Appl. Phys. 10[11] (1971) 1520.
39. N. Nanba, J. Appl. Phys. 53[1] (1982) 695-698.
40. S.R. Elliott, Adv. Phys. 36[2] (1987) 135-217.
41. L.I. Nyrkova, S.H. Polyakov, S.O. Osadchuk, S.L. Mel'nychuk, and N.O. Hapula, Mater. Sci. 47[5] (2012) 683-688.